Energy Advances

ROYAL SOCIETY OF CHEMISTRY

PERSPECTIVE

View Article Online
View Journal | View Issue

Cite this: *Energy Adv.*, 2023, 2, 280

Progress on 2D–2D heterostructured hybrid materials for efficient electrocatalysis

Xia Long, *[a] Lihua Zhang,[ab] Zheng Tan[a] and Bowei Zhou[a]

Received 17th November 2022,
Accepted 24th December 2022

DOI: 10.1039/d2ya00318j

rsc.li/energy-advances

Two-dimensional (2D) materials are widely used in many energy conversion reactions, especially 2D–2D heterostructured hybrid materials that have been extensively investigated in recent years. In this review article, we provide a comprehensive review of the recent research progress on 2D–2D hybrid materials, starting from the introduction of these emerging hybrids. Then, the fabrication strategies are discussed with their pros and cons. Furthermore, the techniques, especially those for heterointerface characterization, are highlighted. Afterward, the applications of these 2D–2D heterostructured hybrid materials in energy conversion reactions with representative examples in the last five years are discussed and summarized. Finally, a summary and perspectives for realizing the rational design and synthesis of 2D–2D hybrids as advanced electrocatalysts towards active and stable energy conversion reactions are provided.

Introduction

Developing renewable green energy sources is one of the most critical topics in material- and energy-related fields nowadays, due to the growing demand for energy and increasing concerns regarding environmental pollution problems.[1,2] Meanwhile, the generation and conversion efficiency of these renewable energy systems largely depend on the effectiveness of the catalysts. Among the developed functional materials for energy conversion reactions, such as hydrogen production *via* water splitting, carbon dioxide reduction to form valuable chemicals and nitrogen reduction to form ammonia, *etc.*, two-dimensional (2D) materials offer unique advantages for these processes due to their large specific surface area, high charge migration rate, adjustable electronic properties, ultralight weight, assembly properties to form heterostructures, high mechanical flexibility, *etc.*[3–8]

Actually, 2D materials have boomed since the successful fabrication of graphene from graphite in 2004 by Novoselvo and co-workers.[9] Since then, many 2D materials have been developed such as MXenes,[10,11] layered double hydroxides

[a] *China-UK Low Carbon College, Shanghai Jiao Tong University, No. 3, Yinlian Road, Lingang, Shanghai, 201306, China. E-mail: x.long@sjtu.edu.cn*
[b] *School of Mechanical Engineering, Shanghai Jiao Tong University, Shanghai, 200240, China*

Xia Long

Xia Long is a tenured Associate Professor at Shanghai Jiao Tong University. She obtained a PhD degree from Peking University in 2013, followed by working at The Hong Kong University of Science and Technology, Fujian Institute of Research on the Structure of Matter, Chinese Academy of Science, and Peking University Shenzhen Graduate School successively. Her current research interests focus on low carbon energy materials and devices, noble metal-free catalysts and devices for energy conversion and storage.

Lihua Zhang

Lihua Zhang is working at Shanghai Jiao Tong University as a postdoctoral researcher. She received her BS degree in Energy Materials from Southern University of Science and Technology in 2016. She received a PhD degree in chemistry from The Hong Kong University of Science and Technology in 2020. Her work focuses on the synthesis of novel and functional nanostructured materials, including perovskite oxides and high-entropy oxide nanoparticles, to explore their potential applications in electrocatalysis.

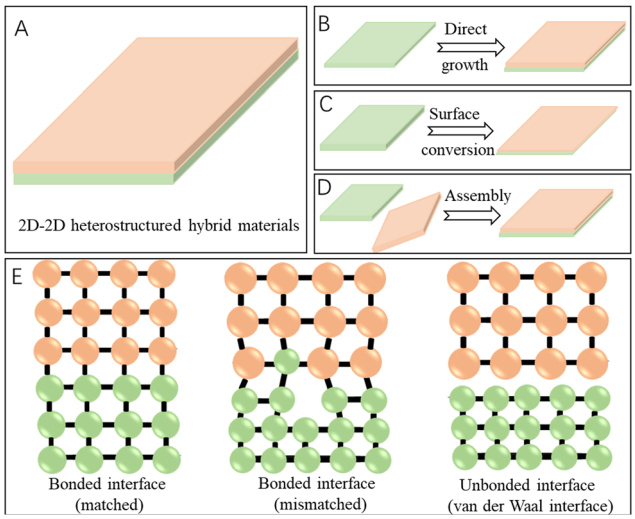

Fig. 1 Schematic illustration of (A) the structure of 2D–2D hybrids, (B–D) 2D–2D hybrid materials made by (B) direct growth, (C) surface conversion, and (D) assembly processes, and (E) the interaction of the two components at the heterointerface.

(LDHs),[8,12,13] transition metal-based dichalcogenides (TMDs),[14–17] black phosphorus,[18–20] covalent-organic frameworks (COFs)[21,22] metal–organic frameworks (MOFs),[23–25] metallenes,[26] borophene,[27] *etc.*[28,29] The unique physical, electronic and chemical properties of these 2D materials mean that they can be expected to have rich and exciting structural and physiochemical properties, making them promising for numerous applications in electronics, sensing, photonics, catalysis, bioengineering, energy harvesting, flexible electronics, *etc.*[3,7,8,30]

Furthermore, based on the unique assembly properties of 2D materials, they can be easily combined with other functional materials to form heterostructured hybrids that would give rise to intriguing features, such as integrating the merits and overcoming the weaknesses of the individual counterparts and even generating new properties or functions.[31–33]

Generally, among all the 2D heterostructured hybrids, the 2D–2D heterostructures have the largest interfacial contact area and the strongest interactions between the two distinct components (Fig. 1A), when compared with the 0D–2D and 1D–2D heterostructures. So, the coupling of the heterointerfaces in the face to face stacking of 2D–2D hybrid materials would be intense, which would further benefit the rearrangement of the electronic structures of the active sites and facilitate the charge transfer during energy conversion reactions, thus contributing to improved catalytic performance.[34,35] Owing to the above-mentioned merits (Table 1), the 2D–2D heterostructured hybrid materials exhibit vast application prospects and a large number of related works have been reported recently. Though there are many excellent review articles on 2D-based materials,[7,33,36–39] a comprehensive review on 2D–2D hybrids with representative examples reported in the last five years and the emphasis on the characterization and effects of heterointerfaces would provide a timely understanding of progress of this promising research field and also promote the development of 2D–2D heterostructured hybrid materials for efficient electrocatalysis towards energy conversion reactions.

Table 1 Summary of the merits of 2D–2D hybrids when compared with other kinds of hybrids

Hybrids	Merits
2D–2D	Large interfacial contact area Strong heterointerface interaction Intense coupling effects Favourable rearrangement of electronic structure Facilitating better charge transfer

This review focuses on the most recently published and instructive studies based on the 2D–2D hybrid catalysts for energy conversion reactions (Fig. 1). Firstly, the fabrication methods of 2D–2D hybrid materials and their unique physicochemical properties will be introduced. Next, the techniques for the characterization of heterointerfaces and their effects will be discussed. Furthermore, the application of the 2D–2D heterostructured hybrid materials in energy conversion catalysis, especially towards hydrogen production *via* water splitting, will be fully demonstrated. Finally, the challenges and perspectives in this promising research area will be expounded based on the current research status.

Zheng Tan

Zheng Tan received his bachelor's degree from School of Mechanical Engineering, Shanghai Jiao Tong University in 2021 and is pursuing his master's degree at China–UK Low Carbon College, Shanghai Jiao Tong University. His research focuses on the surface and interface engineering of noble metal-free catalysts for efficient hydrogen production via water splitting.

Bowei Zhou

Bowei Zhou received his bachelor's degree in New Energy Science and Technology from Northeastern University in 2022 and is pursuing his master's degree at China–UK Low Carbon college, Shanghai Jiao Tong University. His research focuses on key materials and techniques for hydrogen production via seawater electrolysis.

Fabrication of 2D–2D heterostructured hybrid materials

The performance of 2D–2D heterostructured materials in energy conversion catalysis not only depends on their chemical composition, crystal phase, microstructure, and exposed facets, but also on the distribution of each component and the quality of the heterointerface. Therefore, rational design and controlled synthesis methods are critically important for achieving advanced catalytic performance of the as-prepared 2D–2D hybrid materials. Generally, the construction of 2D–2D hybrid materials with heterointerfaces could be classified as growth and conversion processes and assembly processes that will be introduced in detail in this section.

Growth and conversion processes

The growth of 2D–2D heterostructured hybrid materials can be generally described as the growth or formation of the second 2D material on the surface of the primarily synthesized 2D material (the substrate material) (Fig. 1B). Epitaxial growth is one of the most promising approaches for controlled synthesis of materials with heterointerfaces, which refers to a crystalline material grown on the well-defined surface of another crystalline material (the substrate) *via* chemical vapor deposition (CVD) or wet-chemical processes. The deposited crystalline material generally has the same orientation of crystal lattice as the substrate material. Graphene is one of the most widely used 2D substrates for epitaxial growth of 2D–2D hybrid materials such as graphene-TMDs[40,41] and graphene-MoC_2.[42] In addition, h-BN has also been widely used as a 2D substrate material for epitaxial growth of graphene,[43] MoS_2,[44] and WS_2[45] to form the corresponding 2D–2D hybrids.

In addition to carbon materials, transition metal-based 2D materials have also been applied as the substrate for the growth of the second 2D materials. For example, by altering the growth temperature, MoS_2/WS_2 and WS_2/MoS_2 hybrids were synthesized *via* a two-step CVD strategy (Fig. 2A).[46] What is more, it was found that by carefully controlling the temperature (Fig. 2B), a one-step growth was enough for realizing the formation of both vertically stacked and in-plane interconnected heterostructured 2D–2D WS_2/MoS_2 hybrids (Fig. 2C).[47] This synthesis method could be further modified to have scalability and patterning characters for producing large-area 2D–2D hybrids.[48] Besides, many 2D heterostructured hybrids have been reported by using liquid phase epitaxial growth, such as CuS–TiS_2, ZnS–TiS_2, Ni_3S_2–TiS_2, *etc.*[49]

Though many 2D–2D hybrids have been successfully fabricated by epitaxial growth, the selection of the two components is relatively limited, which should have similar lattice structures to lower the degradation of the quality of the interface resulting from the lattice mismatch. In this regard, functionalization of the surface of 2D substrate materials to make them more suitable for the growth of the second 2D material is necessary. Gao *et al.*[50] fabricated Ti_3C_2 nanosheets with a negatively charged surface and then grew Bi_2WO_6 nanosheets on them and successfully constructed Ti_3C_2–Bi_2WO_6 hybrid nanosheets. By similar wet-chemical processes, Xia *et al.*[51] also fabricated a MnO_2–gC_3N_4 hybrid by adsorption of Mn^{2+} ions on the defect- and OH-rich g-C_3N_4 nanosheets.

Different from the growth of the second 2D component, the controlled topotactic conversion of the 2D substrate materials is also an efficient method for the fabrication of 2D–2D hybrids (Fig. 1C). Actually, morphology-retained topotactical conversion processes have been successfully applied to synthesize many

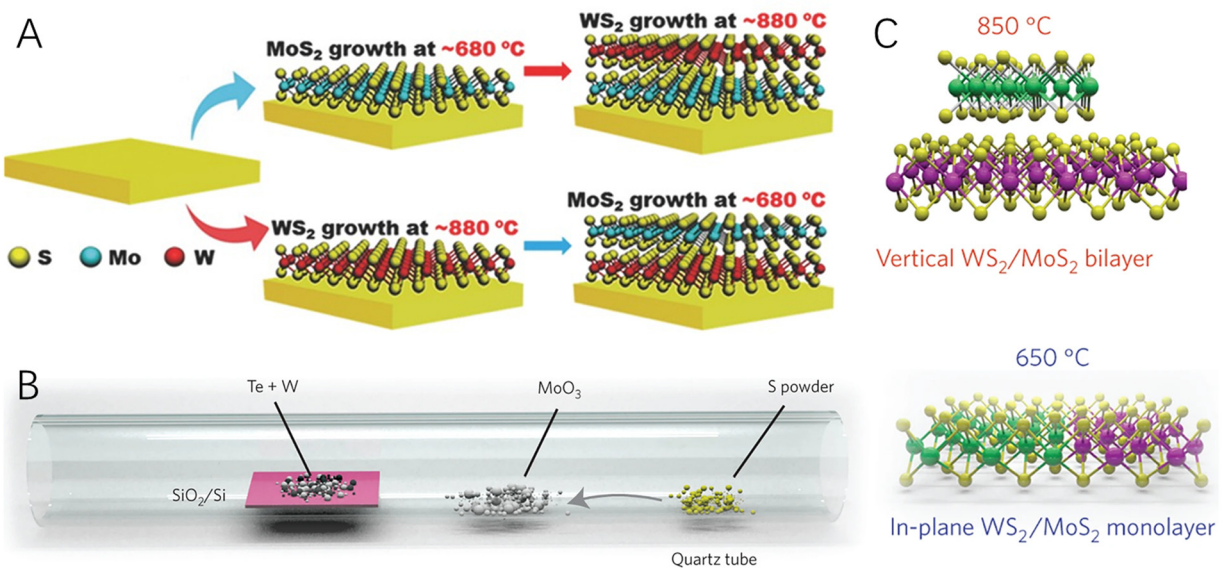

Fig. 2 Schematic illustration of CVD processes for the formation of 2D–2D hybrids. (A) The tunable two-step CVD growth process for the fabrication of MoS_2–WS_2 and WS_2–MoS_2 2D–2D hybrids. Reproduced with permission from ref. 46, copyright Wiley. (B) Schematic of the synthesis process for vertical and in-plane structured WS_2/MoS_2 hybrids. (C) Schematic of the vertically stacked and in-plane WS_2/MoS_2 heterostructures at 850 °C and 650 °C, respectively. Reproduced with permission from ref. 47, copyright Springer Nature.

functional materials to change their physiochemical properties and then catalytic performance.[52–55] For 2D–2D hybrid construction, Qian *et al.* fabricated a $Bi_4Ti_3O_{12}$/I-BiOCl heterostructured hybrid by adding HCl into a $Bi_4Ti_3O_{12}$ nanosheet suspension. The surface of the $Bi_4Ti_3O_{12}$ nanosheets was dissolved in the presence of HCl and the released Bi^{3+} ions near the surface hydrolyzed to BiO^+, which was further transformed to IBiOCl, resulting in the formation of a $Bi_4Ti_3O1_2$/I-BiOCl 2D–2D hybrid.[56] Recently, *via* an *in situ* topotactic hydrothermal transformation process, Shi *et al.* constructed a Cu_2S/$Zn_{0.67}Cd_{0.33}S$ hybrid nanosheet with a 2D–2D atomic level in-plane heterointerface by using 2D CuZnCdAl LDH as the precursor.[57]

Assembly processes

Distinct from the above-mentioned growth or conversion processes, the formation of 2D–2D hybrids was achieved *via* assembly processes generally through the following steps: first, the two 2D components were designed and synthesized separately and then these two pre-synthesized 2D materials were combined together through assembly processes (Fig. 1D). In contrast to the epitaxial growth of 2D–2D hybrids that have a lattice matching constraint, the 2D–2D heterostructures were made by assembly processes often attracted by much weaker electrostatic or van der Waals forces, enabling much more selection space for the construction of 2D–2D hybrids (Fig. 1E).[58,59] Moreover, although the force is relatively weak, the coupling effects between the two 2D components around the interface are still strong enough to affect the re-organization of the electronic structure and then mediate the catalytic performance of the hybrid material for energy conversion catalysis.

Considering that both the $CrSe_2$ and Ti_3C_2 MXene are advanced energy storage materials with 2D layered structures, Raj *et al.* constructed a $CrSe_2$/Ti_3C_2 MXene 2D/2D hybrid by a facile assembly process. The as-prepared hybrids showed a promising energy storage property owing to the increased number of active sites and improved electrochemical stability arising from the synergistic interplay effect triggered by fast ionic/electronic transportation, reduced agglomeration and volume expansion.[60] Recently, Chen *et al.* reported an LDH-birnessite hybrid by a self-assembly of exfoliated LDH nanosheets and birnessite microplates, by taking advantage of the positively charged LDH and negatively charged birnessite and the 2D characters of these two components that readily formed a film.[61] The coupling of the two components at the atomic level allows the formation of a built-in electric field in the hybrid, which contributed to lowering the overpotential of the OER catalysed by this heterostructured hybrid catalyst. Actually, a variety of advanced 2D–2D materials have been successfully synthesized by this route, such as WO_3-$ZnIn_2S_4$,[62] black phosphorus-Bi_2WO_6,[63] Fe_2O_3/g-C_3N_4,[64] metal-free phosphorene (FP)/graphitic carbon nitride,[65] *etc.*

In addition to the low temperature assembly process, 2D–2D hybrids were also prepared *via* the assembly of two components under hydrothermal conditions, to further enhance the coupling of the two materials.[66,67] More recently, Ju *et al.* assembled an LDH with ppy to form an organic–inorganic 2D–2D hybrid of LDH-ppy *via* two steps. Firstly, the negatively charged pyrrole monomer was intercalated into the interlayer of the LDH nanosheets, where they were further polymerized to form a 2D ultrathin film by ultraviolet illumination,[68] suggesting the universality of the assembly process for the fabrication of 2D–2D hybrid materials with various chemical compositions.

Besides wet-chemical assembly processes, the solid state sintering process has also been proven to be an effective approach for the construction of 2D–2D heterostructured materials. For example, Xu *et al.* mixed Bi_4NbO_8Cl and g-C_3N_4 nanosheets together by ball-milling and then annealed the mixture in air. The as-prepared Bi_4NbO_8C–g-C_3N_4 showed a clear heterointerface, suggesting the 2D–2D heterostructure of the hybrid.[69] Similarly, a $Bi_4Ti_3O_{12}$–$Ni(OH)_2$ 2D–2D hybrid was also reported by the solid state sintering process.[70] Though there is no lattice matching constraint for the selection of the two 2D components to form the 2D–2D hybrid *via* solid state sintering methods, they should be chemically and structurally stable during the high temperature annealing procedures. What is more, the interface adhesion in these 2D–2D hybrids is relatively weak, which would probably result in the deterioration of the heterointerface during the catalytic performance evaluation. Therefore, rationally modifying the surface of the 2D materials to consolidate the heterointerface with electrostatic, van der Waals force or even covalent bonding would improve the stability of the 2D–2D hybrid catalysts.

Though the above-mentioned assembly method could produce a large quantity of 2D–2D hybrid materials, they cannot realize the fabrication of large-area 2D–2D hybrids that maintain the intrinsic properties of the two components, while producing pristine interlayer heterointerfaces. Therefore, Kang *et al.*[59] developed a programmed vacuum stack process (PVS) that could generate wafer-scale 2D–2D hybrid films with a very high level of spatial uniformity and pristine interfaces (Fig. 3). The chemical composition and properties of these 2D–2D hybrid films could be designed at atomic scale using layer-by-layer assembly of the 2D building blocks under a vacuum. What is more, the as-prepared large-scale hybrid films were detachable, suspendable and compatible with water or other surfaces, enabling the integration of the prepared 2D–2D hybrid materials with advanced optical and mechanical systems.

In summary, the growth and conversion methods for preparing 2D–2D hybrid materials start from the synthesis of the 2D substrate materials, and then the second 2D materials are *in situ* grown or formed *via* topotactic conversion. Therefore, this method would be scalable for constructing many different kinds of 2D–2D hybrid materials with relatively strong interface interaction. What is more, the 2D–2D hybrids constructed *via* the *in situ* CVD process generally have high quality heterointerfaces that are even suitable for applications in electronics, though expensive facilities are required, while the assembly process is the most universal method to fabricate 2D–2D hybrids by using the two 2D materials that have been synthesized separately as the building blocks. Therefore, the 2D–2D hybrids made by the assembly method feature relatively larger

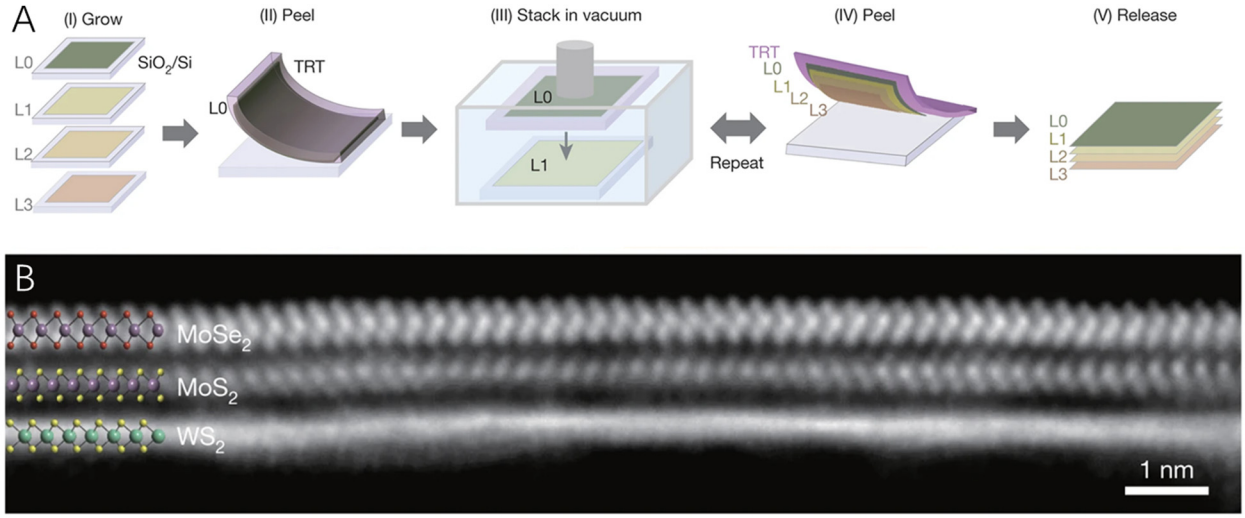

Fig. 3 (A) A schematic of the programmed vacuum stack (PVS) process. (B) The cross-sectional STEM image of a $MoSe_2/MoS_2/WS_2$ film with the electron beam aligned with the armchair axis of $MoSe_2$ (top) and MoS_2 (middle). Reproduced with permission from ref. 59, copyright Springer Nature.

interlayer spacings and more defects, which could benefit the mass/charge transport and provide more active sites during the electrochemical processes. To further realize the uniform hybridization, and then enhance the catalytic performance of the 2D–2D hybrids *via* the assembly processes, the quality and the surface charge of the two 2D building blocks, and the assembly conditions such as temperature, stirring speed, dispersing agent, *etc.* should be well controlled.

Characterization and roles of heterointerfaces

The techniques for characterization of heterointerfaces are vital to guarantee their quality and figure out the role of the interface for catalysis and then promote the development of heterostructured hybrid materials with tailored interfacial structures and properties. Therefore, to fully understand the critical roles of the heterointerfaces and to further improve the overall performance of the hybrids, it is of great importance to obtain accurate information about the microscopic structures and properties of the heterointerfaces by applying reliable characterization techniques.

Electron microscopy techniques such as scanning electron microscopy (SEM) and transmission electron microscopy (TEM) are powerful and extensively used for visualization of the surface of materials at the nanometer scale. However, they could not provide the critical information of the heterointerface of hybrid materials. However, high resolution TEM (HRTEM) that could achieve atomic resolution, when coupled with the focused ion beam lithography (FIB) technique, is a widely used tool for getting the lattice alignment at the heterointerfaces of the 2D–2D hybrid materials. For example, the interface of $Cu_{1.94}S$–CdS 2D–2D nanoplates has been well observed by HRTEM, which showed well-aligned lattice fringes of $Cu_{1.94}S$ (800) and CdS (100) planes.[71] The boundary between TiS_2–CuS heterostructured nanoplates was also characterized by HRTEM and SAED,[49] suggesting the universality of this technique for investigating the interfaces of heterostructured materials.

X-ray photoelectron spectroscopy (XPS) is a useful surface sensitive spectroscopic technique to determine the elemental composition of materials. For the 2D–2D hybrids, the coupling effects arising from the close contact of two distinct materials at the heterointerface would change the electronic configuration of the material, which could be identified by XPS. What is more, the interaction between the two materials would change the surface potential of the hybrid, which could be well characterized by Kelvin probe force microcopy (KPFM). Specifically, KPFM gives precise information on the work function distribution of the materials and the interfacial interaction between the 2D materials. For example, MoS_2/WS_2 heterojunction arrays have been electrically characterized by using conducting atomic force microscopy (CAFM) and the surface potentials of MoS_2 and WS_2 layers were measured by KPFM, which showed a built-in field at the interface to align the Fermi level.[72] Recently, due to the structural compatibility of Bi_2WO_6 and Bi_2O_2S, both of which were 2D semiconductors sharing a similar structural unit of a $[Bi_2O_2]^{2+}$, Xing *et al.*[73] fabricated an ultrathin nanosheet with a tightly bonded 2D–2D heterojunction between the two components by facilely joining the $[Bi_2O_2]^{2+}$ and $[S]^{2-}$ slices (Fig. 4A). The as-prepared Bi_2WO_6–Bi_2O_2S 2D–2D hybrid not only extended light absorption but also significantly enhanced photo(electro)chemical water splitting efficiencies due to the close bonding-promoted interfacial charge separation that has been observed by *in situ* KPFM (Fig. 4B and C).

Though HRTEM gives lattice information and KPFM provides the work function distribution of hybrid materials, they could not determine the exact elemental location around the heterointerface, which is critically important for identifying the boundary of the heterointerface and then facilitating the investigation of the critical roles of the heterointerface for

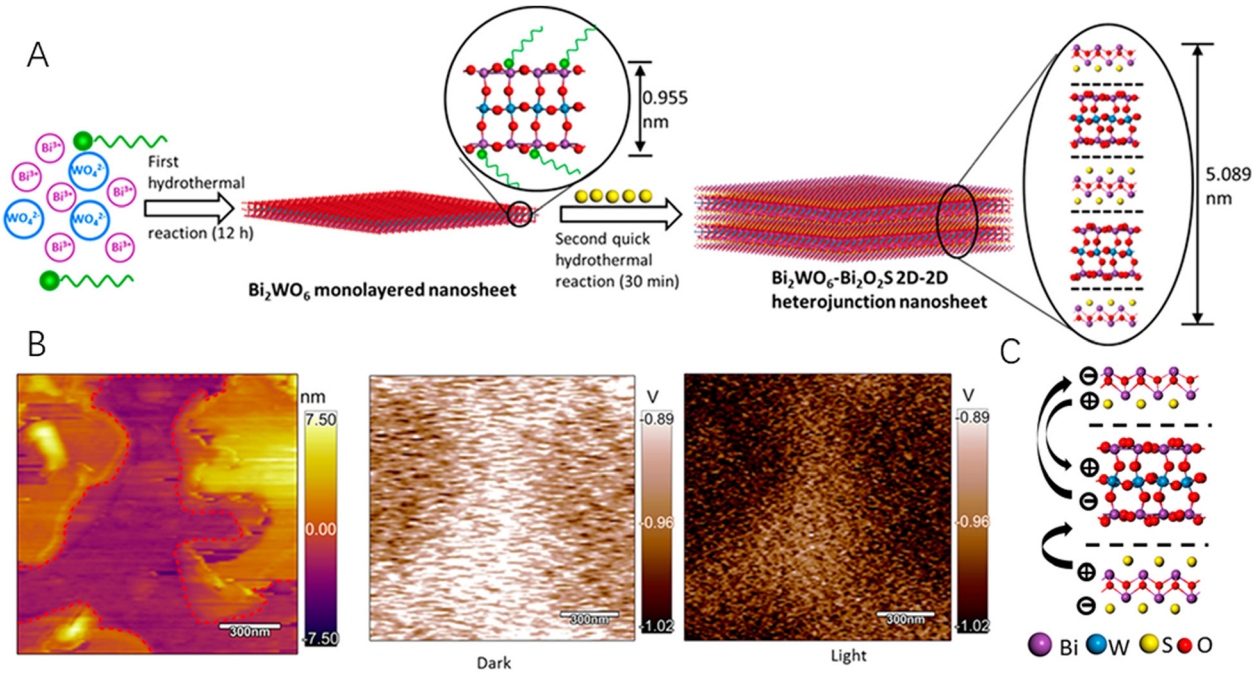

Fig. 4 (A) Schematics of the hydrothermal synthesis process and the transformation process from the monolayered Bi_2WO_6 nanosheet to the Bi_2WO_6-Bi_2O_2S 2D–2D heterojunction nanosheet. (B) The AFM and KPFM images in the dark and under illumination of Bi_2WO_6–Bi_2O_2S nanosheets. (C) Schematics of the charge flow direction in a 2D–2D heterojunction. Reproduced with permission from ref. 73, copyright ACS.

energy conversion catalysis. Electron tomography (CT), which could provide the three-dimensional structure of complex materials in nanometer resolution, is powerful for the characterization of heterostructured catalytic materials, especially the scanning transmission electron microscopy (STEM). STEM is one of the most widely used imaging modes that avoids the appearance of diffraction-related artifacts and is also highly sensitive to the chemical composition of the material. Therefore, it has been rapidly developed as a powerful technique for the characterization of heterostructured catalytic systems,[74] especially the 2D–2D hybrid catalysts. For example, the heterointerface of Bi_2Te_3 with a six-fold symmetry and FeTe with a four-fold symmetry was clearly observed by spherical aberration-corrected STEM.[75] Both the high-angle annular dark field (HAADF, Fig. 5A) and annular bright field (Fig. 5B) images have high contrast with significant sensitivity to the atomic number and thus provide robust visibility of both light and heavy atoms. From the high-magnification HAADF image (Fig. 5C), the Bi_2Te_3 and FeTe were found to be separated by a van der Waals gap with their own lattices undisrupted, confirming the van der Waals epitaxial growth of this 2D–2D hybrid material. Similarly, through atomic-resolution HAADF-STEM, a continuous lattice fringe without any grain boundary or misorientation in a lateral WSe_2–MoS_2 heterohybrid was also clearly observed[76] and the distribution of Mo and W atoms around the heterointerface could be well determined due to the distinct weights of the two elements, suggesting that powerful STEM provides both the structural and chemical information of the heterointerface of 2D–2D hybrid materials.

Though there are many powerful techniques that could provide some important information on the heterointerfaces and many *in situ*/*operando* techniques that could visualize the dynamic behaviours of the catalyst surface, there are few techniques that could track the real time change of heterointerfaces during the catalytic reaction process. What is more, the complexity of the 2D–2D hybrid catalysts would further make the revelation of the effects of the heterointerfaces difficult. Therefore, to determine the critical role of the heterointerfaces in the catalytic performance of the 2D–2D hybrid materials, the coupling of many advanced *in situ* characterization techniques should be developed and a facile synthesis approach for controlled fabrication of well-designed 2D–2D hybrid materials that have relatively simple structures and chemical compositions would also be critically important.

Application of 2D–2D hybrid materials for energy conversion reactions

As mentioned above, 2D materials offer unique merits to energy conversion catalysis due to their large specific surface area, high charge migration rate, tuneable electronic properties, ultralight weight, assembly properties and high mechanical flexibility. What is more, the 2D–2D hybrids with heterostructures and heterointerfaces could further overcome many drawbacks of the single component 2D materials. For energy conversion reaction catalysis, the coupling of the two components at atomic level was found to enhance the activity of the catalytic material,[77] optimize the electronic structure of active

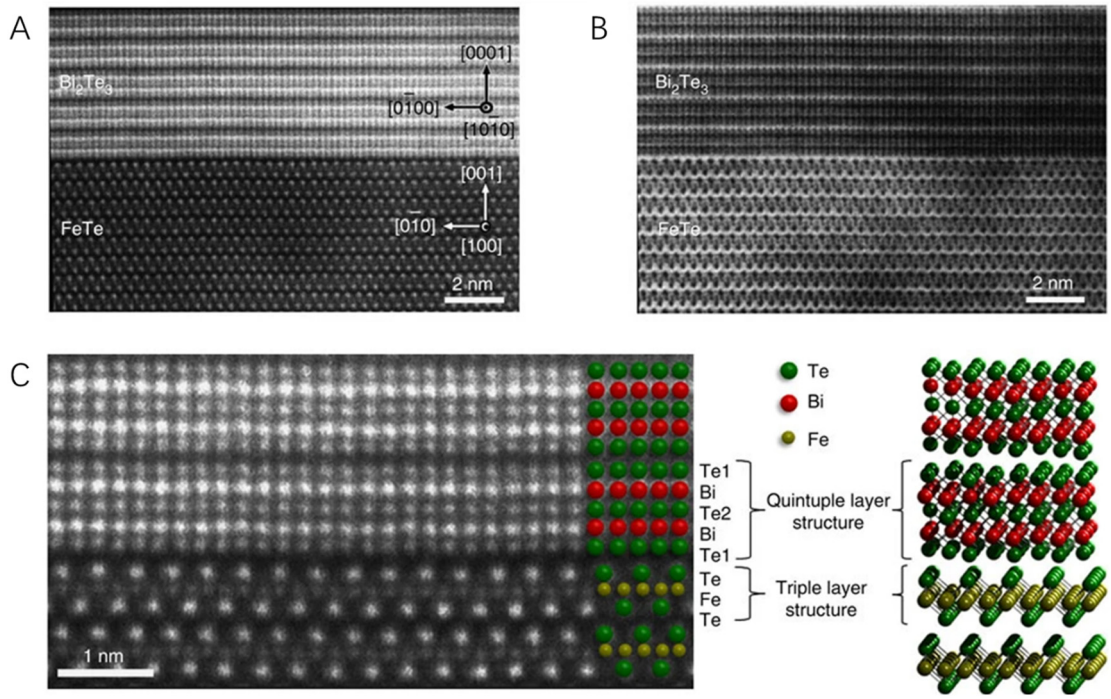

Fig. 5 The scanning transmission electron microscopy micrographs of a Bi_2Te_3/FeTe heterostructure. (A) The HADDF image. (B) The annular bright field image. (C) The higher-magnification HADDF image showing the atomically sharp interface between Bi_2Te_3 and FeTe. Reproduced with permission from ref. 75, copyright Springer Nature.

ions and also accelerate the electron transport processes, all of which would contribute to the enhanced inherent catalytic activity of the 2D–2D hybrid materials.[78] Actually, the advanced 2D–2D hybrids have been widely applied in diverse energy conversion reactions that will be fully discussed with typical examples reported in the last five years in this section.

Hydrogen produced by water splitting is one of the most promising alternatives to replace the fossil fuels, owing to its high energy density (142 MJ kg^{-1}), zero-carbon combustion production and eco-friendly synthesis route.[79,80] For realizing efficient hydrogen production, effective catalysts are critically important and should possess a low overpotential, fast reaction kinetics and good long-term stability in practical applications. Early in 2014, Long *et al.*[81] reported a reduced graphene oxide (rGO) intercalated NiFe LDH 2D–2D hybrid as an efficient OER catalyst in alkali solutions. The direct contact of the highly conductive rGO and OER active NiFe LDH at the atomic level greatly enhanced the charge transfer properties and accelerated the OER kinetics. Later, a superlattice of alternately stacked GO-LDH and rGO-LDH hybrids was further synthesized and applied as both the cathode and anode, which exhibited advanced full water splitting performance that could be driven by a commercial 1.5 V AA battery.[82] What is more, many other 2D materials such as MXenes, TMDs, *etc.* coupled with 2D carbon (graphene, graphene oxides, and rGO) have also been reported, which showed much improved catalytic performance for hydrogen production *via* water splitting, due to the increased active sites and accelerated mass transfer arising from the support of 2D carbon that inhibited the self-stacking of the catalytic active 2D materials and the much enhanced conductivity that improved the charge transfer.[83–88]

In addition to carbon materials, transition metal-based 2D nanomaterials have also been coupled with 2D black phosphorus to construct efficient 2D–2D heterostructured catalysts for water splitting.[89–91] Mei *et al.*[92] reported heterostructured $Ni(OH)_2$-black phosphorus (BP) hybrid nanosheets (BNHNSs) by combining the liquid-exfoliated and mildly oxidized BP with wet-chemical synthesized $Ni(OH)_2$ nanosheets (Fig. 6A). According to the charge density difference (CDD) and electron localization function (ELF) maps (Fig. 6B), an interfacial charge transfer from the 2D $Ni(OH)_2$ nanosheets to the 2D BP nanosheets at the heterointerface could be clearly observed, leading to a favourable electronic structure of the as-prepared BNHNSs. What is more, the adsorption properties of BNHNSs were also found to be desirable for intermediates of alkaline water splitting reactions. Therefore, when applied as an OER catalyst, the 2D–2D BNHNS heterostructured hybrid exhibited excellent catalytic performance with a low overpotential, fast reaction kinetics (Fig. 6C) and long-term stability (Fig. 6D).

The combination of two 2D materials, both of which have excellent redox characters that could work as electrocatalysts, have attracted much attention. For example, Shinde *et al.*[93] developed a $MoTe_2/Ti_3C_2T_x$ 2D–2D hybrid that exhibited efficient HER activity in acidic solutions. The overpotential for attaining the current density of 10 mA cm^{-2} was as low as 293 mV and the Tafel slope was 65 mV dec^{-1}, which was much lower than the two single component counterparts. Based on the analysis of the electronic density of states (DOS), charge

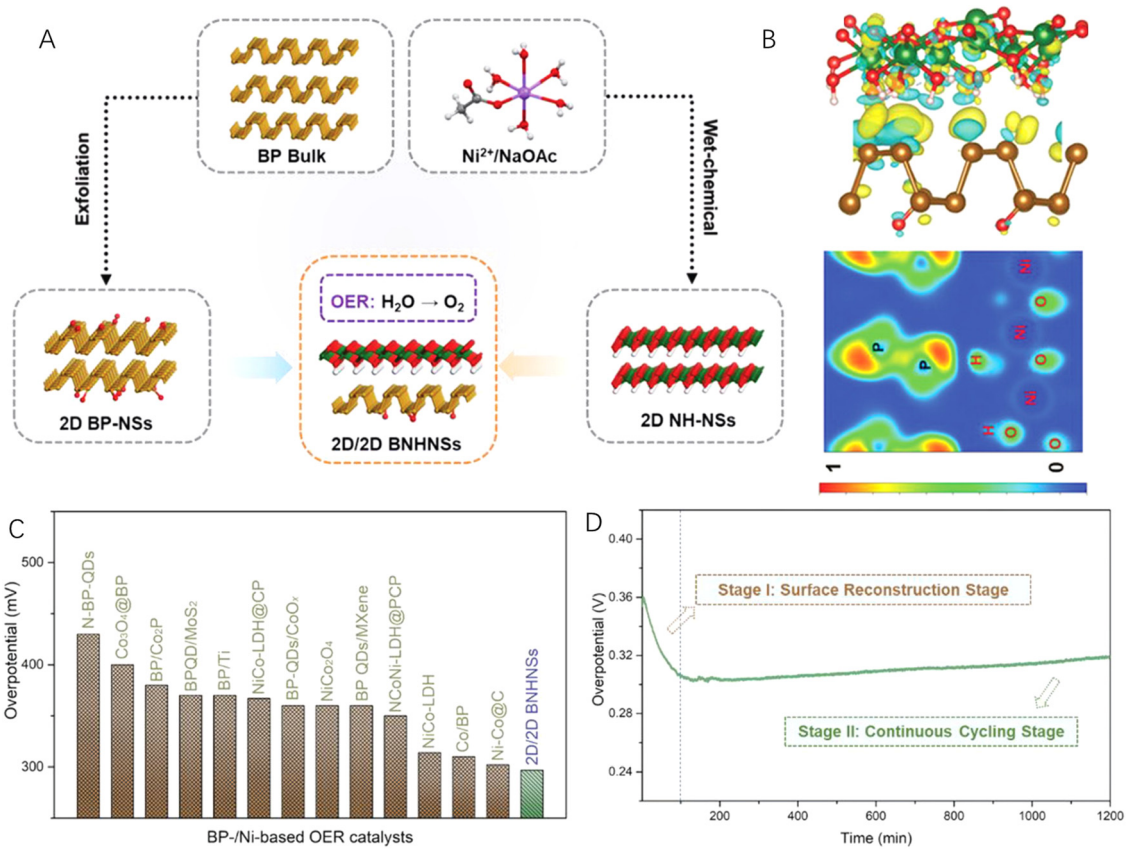

Fig. 6 (A) Schematic illustration of the synthesis of 2D–2D heterostructured nanosheets (BNHNSs) by coupling 2D $Ni(OH)_2$ nanosheets (NH-NSs) and 2D black phosphorus (BP) nanosheets (BP-NSs). (B) The charge density difference and electron localization function maps of 2D–2D BNHNSs. (C) Comparison of the overpotentials with those of the reported electrocatalysts at 10 mA cm^{-2}. (D) Time-dependent overpotential curve of the 2D–2D BNHNSs catalyst in KOH for 1200 min. Reproduced with permission from ref. 92, copyright Wiley.

transfer, and charge density plot, the authors found that an improvement in electronic density states near the Fermi energy for the hybrid system due to orbital hybridization increased the conductivity of the hybrid material. More recently, Chen *et al.*[61] reported a LDH-birnessite hybrid that realized the direct contact of two OER active species of brucite layer of LDH and MnO_x layer of birnessite at the atomic level (Fig. 7A). They found an electron transfer from Ni sites to both the in-plane Fe site and through-plane Mn sites, which not only greatly idealized the electronic structure of the three catalytic active sites (Fe and Ni in LDH and Mn in birnessite, Fig. 7B), but also created a built-in electric field (Fig. 7A) that accelerated the charge transfer during the OER process, hence greatly increasing the reaction kinetics of the alkali OER (Fig. 7C and D). The as-prepared 2D–2D hybrid solved the instability problem of LDH and the low activity of birnessite together, leading to an excellent OER performance with both high activity and long-term stability even under industrial alkali water splitting conditions (Fig. 7E).[61] Similarly, transition metal-based LDH-TMDs with different chemical compositions,[94] LDH-Mxenes,[95–102] MXene-TM sulphides,[103] and LDH-LDH[104] have been successfully synthesized and all of them showed improved catalytic performance towards water splitting, due to the synergistic effect arising from the coupling of two components at the heterointerface.[105,106] However, despite much progress on the fabrication of 2D–2D hybrid materials towards efficient water splitting and many of them even showing superior activity under industrial alkali water splitting conditions, the long-term stability and durability the 2D–2D hybrid catalysts should be further improved and evaluated to meet the requirements of practical applications.

In addition to the production of green hydrogen *via* water splitting, efficient CO_2 reduction (CO_2R) could mitigate the environmental pollution problems, while generating valuable chemicals. However, efficient CO_2R is still challenging for realizing high activity, selectivity and stability, in which, the advanced catalysts are critically important. Due to the above-mentioned structural merits, 2D–2D heterostructured hybrid materials have promising potential as advanced CO_2RR catalysts.[107] For example, Gu *et al.* reported an ultrathin conjugated metalloporphyrin COF-graphene van der Waals heterostructured hybrid material for electrocatalytic CO_2 reduction. The strong electronic coupling between the van der Waals layers accelerated the dynamics of the CO_2 conversion process, leading to advanced conversion efficiency with high CO selectivity.[108]

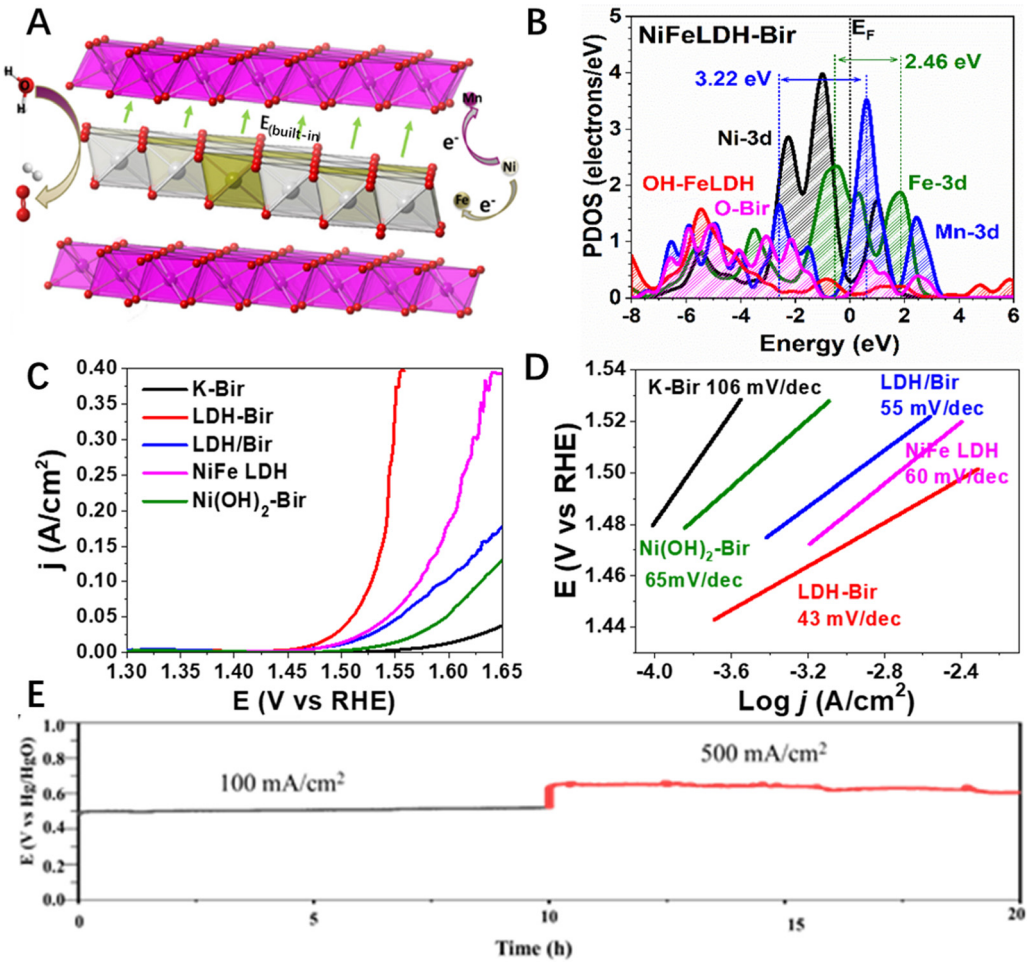

Fig. 7 (A) Schematic illustration the built-in electric field in the LDH-Bir 2D–2D hybrid. (B) PDOS of LDH-Bir, (C) lsv and (D) Tafel plots of LDH-Bir and the control catalysts, and (E) long term stability of LDH-Bir under the industrial alkali water splitting conditions. Reproduced with permission from ref. 61, copyright Wiley.

However, due to the strong reductive reaction conditions of the CO_2RR, the transition metal-based active species would easily be reduced, which would result in the change of both the physiochemical properties and microstructures of the catalysts and hence deteriorate the catalytic performance of the materials. For example, Shen *et al.* found that the CuS–Bi_2S_3 heterojunction would be *in situ* reconstructed to Cu-doped bismuth (CDB) during the CO_2 reduction reaction, though the as-formed CDB also exhibited CO_2RR catalytic performance with an industrially compatible current density of -1.1 A cm^{-2} and high formate selectivity.[109] Therefore, the stability of the 2D–2D hybrids under the CO_2RR conditions should be paid more attention.

Actually, many strategies have been developed to stabilize the CO_2RR catalysts under the highly reductive conditions such as doping and surface/interface engineering[110–114] and rational construction of 2D–2D heterostructures is one of the promising methods. For example, Cai *et al.*[115] reported metallic copper–Cu_xOF 2D hybrid nanoplates for the CO_2RR (Fig. 8A–C). The authors found that the Cu/Cu_xOF 2D–2D hybrid surface showed a strong perturbation of the electronic distribution (Fig. 8D) and the Cu-3d orbitals were located at a position close to the Fermi level (Fig. 8E), suggesting a higher d-band centre and thus an improved electroactivity. When applied as the CO_2RR catalysts, the prepared Cu/Cu_xOF 2D–2D hybrid exhibited excellent CO_2RR activity with high selectivity for acetic acid formation (Fig. 8F). The authors proposed that the F-modified heterointerface could effectively tailor the exposed facets of the metallic Cu nanoparticles, stabilize the oxidized copper active species under the CO_2RR conditions, and purposely induce the s, p–d coupling between the metal and hetero-anions, leading to the selective formation of acetate.

However, despite many successful applications of 2D–2D hybrids for efficient CO_2RR and other energy conversion reactions such as nitrogen fixation,[107,116–119] this promising research area is still in an initial stage that needs more efforts. Revealing the critical roles of heterointerface by using advanced techniques is of importance for directing the rational design of advanced 2D–2D materials and developing a general and controllable construction method to realize the fabrication of targeted 2D–2D heterostructured hybrid materials with particular chemical composition and interface properties is also

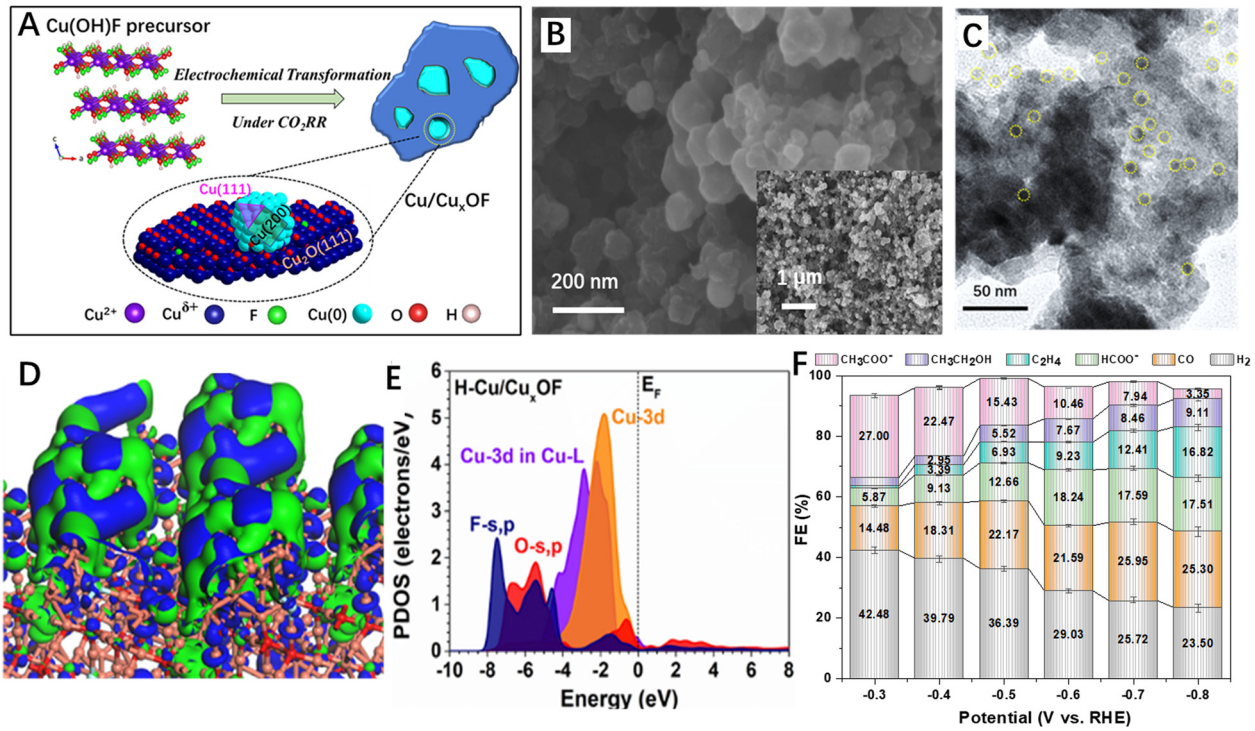

Fig. 8 2D–2D hybrid materials for the CO_2RR. (A) Schematic atomic structures of Cu(OH)F and the transformed Cu/Cu_xOF hybrid. (B) The SEM images with high and low (inset) magnifications of Cu/Cu_xOF 2D–2D nanosheets. (C) TEM images of Cu/Cu_xOF 2D–2D nanosheets. (D) 3D contour plot for electronic distribution and (E) PDOS of Cu/Cu_xOF. (F) FEs of all the products on Cu/Cu_xOF at various applied potentials. Reproduced with permission from ref. 115, copyright RSC.

Table 2 Summary of the electrocatalytic performance of the most active 2D–2D hybrid catalysts for energy conversion reactions

Catalysts	Performance	Ref.
LDH-rGO	Alkali OER: η = 210 mV@10 mA cm^{-2}, 1 M KOH, and RT	81
MoS_2–graphene	Acidic HER: η = 137 mV@10 mA cm^{-2}, 0.5 M H_2SO_4, and RT	85
MXene/CN/rGO	Acidic HER: η = 147 mV@10 mA cm^{-2}, 0.5 M H_2SO_4, and RT	88
Black P@NG	Full water splitting, cell voltage of 1.54 V at 10 mA cm^{-2}, 1 M KOH, and RT	89
$CoFeO_x$-black P	η(OER) = 266 mV@10 mA cm^{-2}, η(HER) = 88 mV@10 mA cm^{-2}, 1 M KOH, and RT	91
Black P-Ni$(OH)_2$	Alkali OER: η = 297 V @10 mA cm^{-2}, 1 M KOH, and RT	92
MXene-LDH	Alkali OER: η = 298 V @10 mA cm^{-2}, 1 M KOH, and RT	96
LDH-LDH	Full water splitting, cell voltage of 1.59 V at 10 mA cm^{-2}, 1 M KOH, and RT	104
TMD-LDH	Full water splitting, cell voltage of 1.49 V at 10 mA cm^{-2}, 0.1 M KOH, and RT	106
$MoTe_2/Ti_3C_2T_x$	Acidic HER: η = 293 mV@10 mA cm^{-2}, 0.5 M H_2SO_4, and RT	93
LDH-Bir	Industrial alkali OER: 0.6 V *vs.* Hg/HgO, 6 M KOH, 85 °C	61
Co-COF/graphene	CO_2RR: 8.2 mA cm^{-2} in H cell, FE(CO) = 97%, 191 mA cm^{-2} in flow cell, FE(CO) = 99%	108
Cu-Cu_xOF	CO_2RR: FE(acetic acid) = 27%, −0.3 V	115
MoS_2/C_3N_4	NRR: NH_3 yield = 18.5 μg h^{-1} mg^{-1}, FE (−0.3 V) = 17.8%	117
CuSe/g-C_3N_4	CO_2RR: FE(CO) = 85.28%, −1.2 V	118

Note: RT means room temperature.

critical for achieving efficient energy conversion with high activity, selectivity and stability.

Summary and perspectives

The 2D–2D heterostructured hybrid materials have the largest interfacial contact area and the strongest interactions between the two 2D components, resulting in strong coupling effects that would influence the electronic structure of the active sites and the charge transfer character during energy conversion reactions. In this review article, we focus on the most recently reported and instructive studies based on the 2D–2D hybrid catalysts for energy conversion reactions, including the fabrication methods, characterization techniques and applications in energy conversion reactions, particularly in water splitting (Table 2).

Despite the considerable achievements in the design and application of 2D–2D hybrid materials for energy conversion reactions, there are still many challenges ahead in this

promising research area. (1) There is a lack of a facile and economic method for the preparation of large scale and high quality 2D–2D hybrid materials with controlled chemical compositions, sizes and microstructures. (2) The synergistic effects between the two 2D components are complicated; however, they are critically important for understanding the roles of the heterointerface in catalysis. So, advanced characterization techniques, especially the *in situ*/*operando* techniques that could provide the real time information on the structural and compositional evolution of 2D–2D heterostructured hybrid materials during the catalysis processes and rationally designed and precisely controlled 2D–2D hybrid systems need to be developed. (3) Theoretical simulations such as DFT with accurate models should be carried out for understanding the reaction mechanism, which could couple with high throughput screening and machine learning to promote a better construction of 2D–2D hybrid materials to meet the requirements of targeted reactions. (4) Fabrication methods of free-standing and large scale 2D–2D heterostructured hybrid material-based electrodes need to be developed to guarantee the high activity and increase the durability of the catalysis reactions under practical application conditions, and hence close the huge gap between the laboratory work and commercialization.

Conflicts of interest

There are no conflicts to declare.

Acknowledgements

The authors appreciate financial support from Shanghai Jiao Tong University (No. WH220828001, ZXDF280001) and Shenzhen Science and Technology Innovation Commission (JCYJ2019080 8155413194).

References

1 S. Chu and A. Majumdar, *Nature*, 2012, **488**, 294.
2 C. Zhao, *Carbon Neutrality*, 2022, **1**, 2.
3 D. H. Deng, K. S. Novoselov, Q. Fu, N. F. Zheng, Z. Q. Tian and X. H. Bao, *Nat. Nanotechnol.*, 2016, **11**, 218.
4 J. Di, C. Yan, A. D. Handoko, Z. W. Seh, H. M. Li and Z. Liu, *Mater. Today*, 2018, **21**, 749.
5 M. Nasilowski, B. Mahler, E. Lhuillier, S. Ithurria and B. Dubertret, *Chem. Rev.*, 2016, **116**, 10934.
6 V. Nicolosi, M. Chhowalla, M. G. Kanatzidis, M. S. Strano and J. N. Coleman, *Science*, 2013, **340**, 1420.
7 C. L. Tan, X. H. Cao, X. J. Wu, Q. Y. He, J. Yang, X. Zhang, J. Z. Chen, W. Zhao, S. K. Han, G. H. Nam, M. Sindoro and H. Zhang, *Chem. Rev.*, 2017, **117**, 6225.
8 X. Long, Z. L. Wang, S. Xiao, Y. M. An and S. H. Yang, *Mater. Today*, 2016, **19**, 213.
9 K. S. Novoselov, A. K. Geim, S. V. Morozov, D. Jiang, Y. Zhang, S. V. Dubonos, I. V. Grigorieva and A. A. Firsov, *Science*, 2004, **306**, 666.
10 M. Naguib, M. Kurtoglu, V. Presser, J. Lu, J. J. Niu, M. Heon, L. Hultman, Y. Gogotsi and M. W. Barsoum, *Adv. Mater.*, 2011, **23**, 4248.
11 V. M. H. Ng, H. Huang, K. Zhou, P. S. Lee, W. X. Que, J. Z. Xu and L. B. Kong, *J. Mater. Chem. A*, 2017, **5**, 3039.
12 D. J. Zhou, P. S. Li, X. Lin, A. McKinley, Y. Kuang, W. Liu, W. F. Lin, X. M. Sun and X. Duan, *Chem. Soc. Rev.*, 2021, **50**, 8790.
13 M. Xu and M. Wei, *Adv. Funct. Mater.*, 2018, **28**, 1802943.
14 H. Xia, Z. D. Shi, C. S. Gong and Y. M. He, *J. Mater. Chem. A*, 2022, **10**, 19067.
15 Q. Fu, J. C. Han, X. J. Wang, P. Xu, T. Yao, J. Zhong, W. W. Zhong, S. W. Liu, T. L. Gao, Z. H. Zhang, L. L. Xu and B. Song, *Adv. Mater.*, 2021, **33**, 1907818.
16 S. Manzeli, D. Ovchinnikov, D. Pasquier, O. V. Yazyev and A. Kis, *Nat. Rev. Mater.*, 2017, **2**, 17033.
17 B. Radisavljevic, A. Radenovic, J. Brivio, V. Giacometti and A. Kis, *Nat. Nanotechnol.*, 2011, **6**, 147.
18 L. K. Li, F. Y. Yang, G. J. Ye, Z. C. Zhang, Z. W. Zhu, W. K. Lou, X. Y. Zhou, L. Li, K. Watanabe, T. Taniguchi, K. Chang, Y. Y. Wang, X. H. Chen and Y. B. Zhang, *Nat. Nanotechnol.*, 2016, **11**, 592.
19 B. S. Li, C. Lai, G. M. Zeng, D. L. Huang, L. Qin, M. M. Zhang, M. Cheng, X. G. Liu, H. Yi, C. Y. Zhou, F. L. Huang, S. Y. Liu and Y. K. Fu, *Small*, 2019, **15**, 1804565.
20 H. Liu, A. T. Neal, Z. Zhu, Z. Luo, X. F. Xu, D. Tomanek and P. D. Ye, *ACS Nano*, 2014, **8**, 4033.
21 J. W. Colson, A. R. Woll, A. Mukherjee, M. P. Levendorf, E. L. Spitler, V. B. Shields, M. G. Spencer, J. Park and W. R. Dichtel, *Science*, 2011, **332**, 228.
22 K. Y. Geng, T. He, R. Y. Liu, S. Dalapati, K. T. Tan, Z. P. Li, S. S. Tao, Y. F. Gong, Q. H. Jiang and D. L. Jiang, *Chem. Rev.*, 2020, **120**, 8814.
23 Y. Peng, Y. S. Li, Y. J. Ban, H. Jin, W. M. Jiao, X. L. Liu and W. S. Yang, *Science*, 2014, **346**, 1356.
24 T. Rodenas, I. Luz, G. Prieto, B. Seoane, H. Miro, A. Corma, F. Kapteijn, F. X. L. I. Xamena and J. Gascon, *Nat. Mater.*, 2015, **14**, 48.
25 U. Khan, A. Nairan, J. K. Gao and Q. C. Zhang, *Small Struct.*, 2022, 2200109, DOI: **10.1002/sstr.202200109**.
26 P. Prabhu and J.-M. Lee, *Chem. Soc. Rev.*, 2021, **50**, 6700.
27 Y. V. Kaneti, D. P. Benu, X. Xu, B. Yuliarto, Y. Yamauchi and D. Golberg, *Chem. Rev.*, 2021, **122**, 1000.
28 X. Wu, S. Xiao, Y. Long, T. Ma, W. Shao, S. Cao, X. Xiang, L. Ma, L. Qiu, C. Cheng and C. Zhao, *Small*, 2022, **18**, 2105831.
29 H. Jin, T. Song, U. Paik and S.-Z. Qiao, *ACC. Mater. Res.*, 2021, **2**, 559.
30 K. L. Huang, C. H. Li, H. Z. Li, G. M. Ren, L. Wang, W. T. Wang and X. C. Meng, *ACS Appl. Nano Mater.*, 2020, **3**, 9581.
31 C. L. Tan, J. Z. Chen, X. J. Wu and H. Zhang, *Nat. Rev. Mater.*, 2018, **3**, 17089.
32 Y. P. Liu, S. Y. Zhang, J. He, Z. M. M. Wang and Z. W. Liu, *Nano-Micro Lett.*, 2019, **11**, 13.

33 J. Mei, T. Liao and Z. Q. Sun, *Energy Environ. Mater.*, 2022, **5**, 115.
34 D. S. Wang, *Chin. J. Catal.*, 2022, **43**, 1380.
35 H. L. Hou, X. K. Zeng and X. W. Zhang, *Sci. China Mater.*, 2020, **63**, 2119.
36 T. Li, T. Jing, D. Rao, S. Mourdikoudis, Y. Zuo and M. Wang, *Inorg. Chem. Front.*, 2022, **9**, 6008.
37 S. Aftab, M. Z. Iqbal, M. W. Iqbal, M. Asghar and H. Ullah, *J. Mater. Chem. C*, 2022, **10**, 14795.
38 S. Chandrasekaran, D. T. Ma, Y. Q. Ge, L. B. Deng, C. Bowen, J. Roscow, Y. Zhang, Z. Q. Lin, R. D. K. Misra, J. Q. Li, P. X. Zhang and H. Zhang, *Nano Energy*, 2020, **77**, 105080.
39 C. Chang, W. Chen, Y. Chen, Y. H. Chen, Y. Chen, F. Ding, C. H. Fan, H. J. Fan, Z. X. Fan, C. Gong, Y. J. Gong, Q. Y. He, X. Hong, S. Hu, W. D. Hu, W. Huang, Y. Huang, W. Ji, D. H. Li, L. J. Li, Q. Li, L. Lin, C. Y. Ling, M. H. Liu, N. Liu, Z. Liu, K. P. Loh, J. M. Ma, F. Miao, H. L. Peng, M. F. Shao, L. Song, S. Su, S. Sun, C. L. Tan, Z. Y. Tang, D. S. Wang, H. Wang, J. L. Wang, X. Wang, X. R. Wang, A. T. S. Wee, Z. M. Wei, Y. E. Wu, Z. S. Wu, J. Xiong, Q. H. Xiong, W. G. Xu, P. Yin, H. B. Zeng, Z. Y. Zeng, T. Y. Zhai, H. Zhang, H. Zhang, Q. C. Zhang, T. R. Zhang, X. Zhang, L. D. Zhao, M. T. Zhao, W. J. Zhao, Y. X. Zhao, K. G. Zhou, X. Zhou, Y. Zhou, H. W. Zhu, H. Zhang and Z. F. Liu, *Acta Phys-Chim Sin*, 2021, **37**(12), 2108017.
40 H. Ago, S. Fukamachi, H. Endo, P. Solis-Fernandez, R. M. Yunus, Y. Uchida, V. Panchal, O. Kazakova and M. Tsuji, *ACS Nano*, 2016, **10**, 3233.
41 X. L. Liu, I. Balla, H. Bergeron, G. P. Campbell, M. J. Bedzyk and M. C. Hersam, *ACS Nano*, 2016, **10**, 1067.
42 C. Xu, S. A. Song, Z. B. Liu, L. Chen, L. B. Wang, D. X. Fan, N. Kang, X. L. Ma, H. M. Cheng and W. C. Ren, *ACS Nano*, 2017, **11**, 5906.
43 W. Yang, G. R. Chen, Z. W. Shi, C. C. Liu, L. C. Zhang, G. B. Xie, M. Cheng, D. M. Wang, R. Yang, D. X. Shi, K. Watanabe, T. Taniguchi, Y. G. Yao, Y. B. Zhang and G. Y. Zhang, *Nat. Mater.*, 2013, **12**, 792.
44 D. Y. Fu, X. X. Zhao, Y. Y. Zhang, L. J. Li, H. Xu, A. R. Jang, S. I. Yoon, P. Song, S. M. Poh, T. H. Ren, Z. Ding, W. Fu, T. J. Shin, H. S. Shin, S. T. Pantelides, W. Zhou and K. P. Loh, *J. Am. Chem. Soc.*, 2017, **139**, 9392.
45 B. Wu, H. H. Zheng, S. F. Li, J. N. Ding, Y. J. Zeng, Z. W. Liu and Y. P. Liu, *Nanoscale*, 2022, **14**, 12447.
46 J. P. Shi, R. Tong, X. B. Zhou, Y. Gong, Z. P. Zhang, Q. Q. Ji, Y. Zhang, Q. Y. Fang, L. Gu, X. N. Wang, Z. F. Liu and Y. F. Zhang, *Adv. Mater.*, 2016, **28**, 10664.
47 Y. J. Gong, J. H. Lin, X. L. Wang, G. Shi, S. D. Lei, Z. Lin, X. L. Zou, G. L. Ye, R. Vajtai, B. I. Yakobson, H. Terrones, M. Terrones, B. K. Tay, J. Lou, S. T. Pantelides, Z. Liu, W. Zhou and P. M. Ajayan, *Nat. Mater.*, 2014, **13**, 1135.
48 J. M. Woods, Y. Jung, Y. J. Xie, W. Liu, Y. H. Liu, H. H. Wang and J. J. Cha, *ACS Nano*, 2016, **10**, 2004.
49 C. L. Tan, Z. Y. Zeng, X. Huang, X. H. Rui, X. J. Wu, B. Li, Z. M. Luo, J. Z. Chen, B. Chen, Q. Y. Yan and H. Zhang, *Angew. Chem., Int. Ed.*, 2015, **54**, 1841.
50 S. W. Cao, B. J. Shen, T. Tong, J. W. Fu and J. G. Yu, *Adv. Funct. Mater.*, 2018, **28**, 1800136.
51 P. F. Xia, B. C. Zhu, B. Cheng, J. G. Yu and J. S. Xu, *ACS Sustainable Chem. Eng.*, 2018, **6**, 965.
52 X. Long, Z. J. Ma, H. Yu, X. Y. Gao, X. Y. Pan, X. X. Chen, S. H. Yang and Z. G. Yi, *J. Mater. Chem. A*, 2016, **4**, 14939.
53 X. Long, H. Lin, D. Zhou, Y. M. An and S. H. Yang, *ACS Energy Lett.*, 2018, **3**, 290.
54 X. Long, G. X. Li, Z. L. Wang, H. Y. Zhu, T. Zhang, S. Xiao, W. Y. Guo and S. H. Yang, *J. Am. Chem. Soc.*, 2015, **137**, 11900.
55 Z. W. Chen, Z. Wang, R. M. Cai, Y. S. Xie, J. Yu, X. Long, B. Yang and S. H. Yang, *Nanoscale*, 2020, **12**, 2472.
56 K. Qian, L. Xia, Z. F. Jiang, W. Wei, L. L. Chen and J. M. Xie, *Catal. Sci. Technol.*, 2017, **7**, 3863.
57 J. J. Shi, S. D. Li, F. M. Wang, L. N. Gao, Y. M. Li, X. R. Zhang and J. Lu, *Dalton Trans.*, 2019, **48**, 3327.
58 Y. Liu, Y. Huang and X. F. Duan, *Nature*, 2019, **567**, 323.
59 K. Kang, K. H. Lee, Y. M. Han, H. Gao, S. E. Xie, D. A. Muller and J. Park, *Nature*, 2017, **550**, 229.
60 K. A. S. Raj, N. Barman, K. Namsheer, R. Thapa and C. S. Rout, *Sustainable Energy Fuels*, 2022, **6**, 5187.
61 Z. W. Chen, M. Ju, M. Z. Sun, L. Jin, R. M. Cai, Z. Wang, L. Dong, L. M. Peng, X. Long, B. L. Huang and S. H. Yang, *Angew. Chem., Int. Ed.*, 2021, **60**, 9699.
62 P. F. Tan, A. Q. Zhu, L. L. Qiao, W. X. Zeng, Y. J. Ma, H. G. Dong, J. P. Xie and J. Pan, *Inorg. Chem. Front.*, 2019, **6**, 929.
63 J. D. Hu, D. Y. Chen, Z. Mo, N. J. Li, Q. F. Xu, H. Li, J. H. He, H. Xu and J. M. Lu, *Angew. Chem., Int. Ed.*, 2019, **58**, 2073.
64 Q. Xu, B. Zhu, C. Jiang, B. Cheng and J. Yu, *Solar RRL*, 2018, **2**, 1800006.
65 J. R. Ran, W. W. Guo, H. L. Wang, B. C. Zhu, J. G. Yu and S. Z. Qiao, *Adv. Mater.*, 2018, **30**, 1800128.
66 D. L. Jiang, T. Y. Wang, Q. Xu, D. Li, S. C. Meng and M. Chen, *Appl Catal B Environ*, 2017, **201**, 617.
67 X. D. Ma, D. L. Jiang, P. Xiao, Y. Jin, S. C. Meng and M. Chen, *Catal. Sci. Technol.*, 2017, **7**, 3481.
68 M. Ju, R. M. Cai, J. Z. Ren, J. X. Chen, L. M. Qi, X. Long and S. H. Yang, *ACS Appl. Mater. Interfaces*, 2021, **13**, 37063.
69 Y. Xu, Y. You, H. W. Huang, Y. X. Guo and Y. H. Zhang, *J. Hazard. Mater.*, 2020, **381**, 121159.
70 X. Q. Liu, Z. P. Zhou, D. L. Han, T. Wang, C. C. Ma, P. W. Huo and Y. S. Yan, *J. Alloy Compd.*, 2020, **816**, 152530.
71 M. D. Regulacio, C. Ye, S. H. Lim, M. Bosman, L. Polavarapu, W. L. Koh, J. Zhang, Q. H. Xu and M. Y. Han, *J. Am. Chem. Soc.*, 2011, **133**, 2052.
72 I. Sharma and B. R. Mehta, *J. Alloy Compd.*, 2017, **723**, 50.
73 Z. Xing, J. Hu, M. Ma, H. Lin, Y. M. An, Z. H. Liu, Y. Zhang, J. Y. Li and S. H. Yang, *J. Am. Chem. Soc.*, 2019, **141**, 19715.
74 A. B. Hungria, J. J. Calvino and J. C. Hernandez-Garrido, *Top. Catal.*, 2019, **62**, 808.
75 Q. L. He, H. C. Liu, M. Q. He, Y. H. Lai, H. T. He, G. Wang, K. T. Law, R. Lortz, J. N. Wang and I. K. Sou, *Nat. Commun.*, 2014, **5**, 4247.

76 M. Y. Li, Y. M. Shi, C. C. Cheng, L. S. Lu, Y. C. Lin, H. L. Tang, M. L. Tsai, C. W. Chu, K. H. Wei, J. H. He, W. H. Chang, K. Suenaga and L. J. Li, *Science*, 2015, **349**, 524.
77 R. Y. Ge, J. J. Huo, M. J. Sun, M. Y. Zhu, Y. Li, S. L. Chou and W. X. Li, *Small*, 2021, **17**, 1903380.
78 H. Wang, J. Qi, N. L. Yang, W. Cui, J. Y. Wang, Q. H. Li, Q. H. Zhang, X. Q. Yu, L. Gu, J. Li, R. B. Yu, K. K. Huang, S. Y. Song, S. H. Feng and D. Wang, *Angew. Chem., Int. Ed.*, 2020, **59**, 19691.
79 X. Li, L. L. Zhao, J. Y. Yu, X. Y. Liu, X. L. Zhang, H. Liu and W. J. Zhou, *Nano-Micro Lett.*, 2020, **12**, 131.
80 F. Dawood, M. Anda and G. M. Shafiullah, *Int. J. Hydrogen Energy*, 2020, **45**, 3847.
81 X. Long, J. K. Li, S. Xiao, K. Y. Yan, Z. L. Wang, H. N. Chen and S. H. Yang, *Angew. Chem., Int. Ed.*, 2014, **53**, 7584.
82 W. Ma, R. Ma, C. Wang, J. Liang, X. Liu, K. Zhou and T. Sasaki, *ACS Nano*, 2015, **9**, 1977.
83 Z. Zhang, P. Z. Liu, Y. H. Song, Y. Hou, B. S. Xu, T. Liao, H. X. Zhang, J. J. Guo and Z. Q. Sun, *Adv. Sci.*, 2022, 2204297.
84 A. Rendon-Patino, A. Domenech-Carbo, A. Primo and H. Garcia, *Nanomaterials*, 2020, **10**, 839.
85 P. Xiong, R. Z. Ma, N. Sakai, L. Nurdiwijayanto and T. Sasaki, *ACS Energy Lett.*, 2018, **3**, 997.
86 G. H. Wu, T. T. Li, Z. L. Wang, M. Z. Li, B. W. Wang and A. G. Dong, *Angew. Chem., Int. Ed.*, 2020, **59**, 20628.
87 C. Tang, L. Zhong, B. Zhang, H. F. Wang and Q. Zhang, *Adv. Mater.*, 2018, **30**, 1705110.
88 H. He, Y. Chen, C. Yang, L. Yang, Q. Jiang and H. Huang, *J. Energy Chem.*, 2022, **67**, 483.
89 Z. K. Yuan, J. Li, M. J. Yang, Z. S. Fang, J. H. Jian, D. S. Yu, X. D. Chen and L. M. Dai, *J. Am. Chem. Soc.*, 2019, **141**, 4972.
90 X. Wang, R. K. M. Raghupathy, C. J. Querebillo, Z. Q. Liao, D. Q. Li, K. Lin, M. Hantusch, Z. Sofer, B. H. Li, E. Zschech, I. M. Weidinger, T. D. Kuhne, H. Mirhosseini, M. H. Yu and X. L. Feng, *Adv. Mater.*, 2021, **33**, 2008752.
91 X. Y. Li, L. P. Xiao, L. Zhou, Q. C. Xu, J. Weng, J. Xu and B. Liu, *Angew. Chem., Int. Ed.*, 2020, **59**, 21106.
92 J. Mei, J. Shang, T. W. He, D. C. Qi, L. Z. Kou, T. Liao, A. J. Du and Z. Q. Sun, *Adv. Energy Mater.*, 2022, **12**, 2201141.
93 P. V. Shinde, P. Mane, D. J. Late, B. Chakraborty and C. S. Rout, *ACS Appl. Energy Mater.*, 2021, **4**, 11886.
94 K. R. G. Lim, A. D. Handoko, S. K. Nemani, B. Wyatt, H.-Y. Jiang, J. Tang, B. Anasori and Z. W. Seh, *ACS Nano*, 2020, **14**, 10834.
95 P. W. Xu, H. H. Wang, J. Liu, X. Z. Feng, W. J. Ji and C. T. Au, *ACS Appl. Mater. Interfaces*, 2021, **13**, 34308.
96 M. Z. Yu, S. Zhou, Z. Y. Wang, J. J. Zhao and J. S. Qiu, *Nano Energy*, 2018, **44**, 181.
97 C. Y. Li, D. D. Zhang, J. Cao, P. F. Yu, M. Okhawilai, J. Yi, J. Q. Qin and X. Y. Zhang, *ACS Appl. Energy Mater.*, 2021, **4**, 7821.
98 C. Y. Hao, Y. Wu, Y. J. An, B. H. Cui, J. N. Lin, X. N. Li, D. H. Wang, M. H. Jiang, Z. X. Cheng and S. Hu, *Mater. Today Energy*, 2019, **12**, 453.
99 C. F. Du, K. N. Dinh, Q. H. Liang, Y. Zheng, Y. B. Luo, J. L. Zhang and Q. Y. Yan, *Adv. Energy Mater.*, 2018, **8**, 1801127.
100 M. Z. Yu, Z. Y. Wang, J. S. Liu, F. Sun, P. J. Yang and J. S. Qiu, *Nano Energy*, 2019, **63**, 103880.
101 M. Yu, J. Zheng and M. Guo, *J. Energy Chem.*, 2022, **70**, 472.
102 Y. Wen, Z. Wei, J. Liu, R. Li, P. Wang, B. Zhou, X. Zhang, J. Li and Z. Li, *J. Energy Chem.*, 2021, **52**, 412.
103 G. Zuo, Y. Wang, W. L. Teo, A. Xie, Y. Guo, Y. Dai, W. Zhou, D. Jana, Q. Xian and W. Dong, *Angew. Chem.*, 2020, **132**, 11383.
104 R. Yang, Y. M. Zhou, Y. Y. Xing, D. Li, D. L. Jiang, M. Chen, W. D. Shi and S. Q. Yuan, *Appl. Catal., B*, 2019, **253**, 131.
105 H. Zhang, G. Q. Shen, X. Y. Liu, B. Ning, C. X. Shi, L. Pan, X. W. Zhang, Z. F. Huang and J. J. Zou, *Chin. J. Catal.*, 2021, **42**, 1732.
106 M. S. Islam, M. Kim, X. Y. Jin, S. M. Oh, N. S. Lee, H. Kim and S. J. Hwang, *ACS Energy Lett.*, 2018, **3**, 952.
107 M. A. Ahsan, T. W. He, J. C. Noveron, K. Reuter, A. R. Puente-Santiago and R. Luque, *Chem. Soc. Rev.*, 2022, **51**, 812.
108 H. Gu, G. Shi, L. Zhong, L. Liu, H. Zhang, C. Yang, K. Yu, C. Zhu, J. Li, S. Zhang, C. Chen, Y. Han, S. Li and L. Zhang, *J. Am. Chem. Soc.*, 2022, **144**(47), 21502.
109 H. Shen, Y. Zhao, L. Zhang, Y. He, S. Yang, T. Wang, Y. Cao, Y. Guo, Q. Zhang and H. Zhang, *Adv. Energy Mater.*, 2022, **13**(1), 2202818.
110 Y. S. Zhou, F. L. Che, M. Liu, C. Q. Zou, Z. Q. Liang, P. De Luna, H. F. Yuan, J. Li, Z. Q. Wang, H. P. Xie, H. M. Li, P. N. Chen, E. Bladt, R. Quintero-Bermudez, T. K. Sham, S. Bals, J. Hofkens, D. Sinton, G. Chen and E. H. Sargent, *Nat. Chem.*, 2018, **10**, 974.
111 D. Wakerley, S. Lamaison, F. Ozanam, N. Menguy, D. Mercier, P. Marcus, M. Fontecave and V. Mougel, *Nat. Mater.*, 2019, **18**, 1222.
112 W. C. Ma, S. J. Xie, T. T. Liu, Q. Y. Fan, J. Y. Ye, F. F. Sun, Z. Jiang, Q. H. Zhang, J. Cheng and Y. Wang, *Nat. Catal.*, 2020, **3**, 478.
113 H. F. Li, T. F. Liu, P. F. Wei, L. Lin, D. F. Gao, G. X. Wang and X. H. Bao, *Angew. Chem., Int. Ed.*, 2021, **60**, 14329.
114 Z. Y. Yin, C. Yu, Z. L. Zhao, X. F. Guo, M. Q. Shen, N. Li, M. Muzzio, J. R. Li, H. Liu, H. H. Lin, J. Yin, G. Lu, D. Su and S. H. Sun, *Nano Lett.*, 2019, **19**, 8658.
115 R. M. Cai, M. Z. Sun, J. Z. Ren, M. Ju, X. Long, B. L. Huang and S. H. Yang, *Chem. Sci.*, 2021, **12**, 15382.
116 G. Z. S. Ling, S. F. Ng and W. J. Ong, *Adv. Funct. Mater.*, 2022, **32**, 2111875.
117 K. Chu, Y. P. Liu, Y. B. Li, Y. L. Guo and Y. Tian, *ACS Appl. Mater. Interfaces*, 2020, **12**, 7081.
118 H. Zhang, T. W. Ouyang, J. M. Li, M. M. Mu and X. H. Yin, *Electrochim. Acta*, 2021, **390**, 138766.
119 K. Wang, Q. P. Wang, K. J. Zhang, G. H. Wang and H. K. Wang, *J. Mater. Sci. Technol.*, 2022, **124**, 202.